CFAR SHIP DETECTION FOR SAR IMAGES UNDER CHANGING WAVE CONDITIONS

João A. Lorenzzetti [1], *Diego X. Bezerra* [2], *Rafael L. Paes* [3]

[1]National Institute for Space Research - INPE, Av. Astronautas, 1758 São José dos Campos, SP, joao.lorenzzetti@inpe.br; [2]Orbty, Parque Tecnológico, São José dos Campos, Rodovia Presidente Dutra, 500, diegoxavier95@gmail.com; [3]Air Force General Staff, Esplanada dos Ministérios, Bloco M, Brasília-DF, rafaelpaesrlp@fab.mil.br

ABSTRACT

We present in this paper the result of an analysis of the effect of wave climate, measured by the Wave Age (WA) parameter, first upon the goodness of fit of the chosen pdf used for the Synthetic Aperture Radar-SAR Ocean clutter and, secondly on the accuracy of Constant False Alarm Rate –CFAR algorithm used for ship detection. The important point of the establishment of the Threshold - T for accepting, or not, a bright pixel as a potential ship is dealt with a suggestion of T adjustment dependent on the WA value. The region of interest–ROI for the study is the Brazilian Northeast coastal and offshore area impacted or related to the large episode of oil spills in 2019.

Key words — Ship detection, Synthetic Aperture Radar, CFAR, Wave age, False alare rate.

1. INTRODUCTION

The use of SAR image data, in various microwave bands, polarizations, spatial resolutions and image modes, for ship or target detection, mostly using the CFAR statistical model, is a consolidated technique [1], [2]. The detection of ships and targets in a SAR image is a very important and useful result for search and rescue operations and safeguard of life at sea, for shipping operations, oil spill monitoring and strategic military uses. The ocean is a very dynamic environment, which is subject to quick changes, particularly in the surface wave magnitude and spectrum, with frequent and randomly distributed wave breaking phenomena. Changes in the surface wind field (in magnitude, direction, duration and fetch) affect the wave field, both at longer wavelengths (swell and wind sea waves) and short scales (gravity-capillary and capillary waves) responsible for the backscatter of microwave radar pulses. These phenomena impact the statistical properties of the radar return making it very difficult the fitting of any pdf of radar sigma-zero values of the radar scene in analysis. It is the objective of this paper to present this problem and to suggest a correcting criterion for the threshold to be used for the chosen pdf and used in the CFAR ship detection algorithm.

2. DATA SET AND METHODS

Data Set

A. SAR images: The SAR images use are Sentinel-1 (S-1) VV- pol in ground range detected (GRD) product format and interferometric wide (IW) swath mode. The images spatial coverage consists of the adjacent oceanic region of Northeast Brazil. The image data set includes a wide time span of the year (from April to November 2019). All the images were radiometrically corrected, land masked, georeferenced, and resampled to 30 m pixel spacing.

B. Auxiliary information: ERA5 reanalysis product [3] was used to provide supplementary oceanic surface wind and wave information for the regions and dates of used SAR images. A comparison of CFAR ship detection results against AIS position of ships was done using a high-temporal-frequency AIS data set (< 3 min), provided free of charge by HisdeSAT/ExactEarth.

Methods

The SAR image in analysis, consisting of 30 m pixels, was sub-divided into tiles, each consisting of 667x667 pixels, equivalent to an area of ~20x20 km. For each image tile we used the ERA5 surface wind and wave spectrum peak period to estimate friction velocity u* (which is related to the wind stress) and peak wave phase speed C_p and, finally the wave age (WA), the ratio C_p/u^*. Each sub-image was then classified as: young wind-sea ($WA \leq 10$); old wind-sea ($10 < WA \leq 35$), or swell ($WA > 35$) [4]. To evaluate the influence of distinct sea environmental conditions on the CFAR algorithm performance, only sub-images representing pure ocean backscattering were selected using the criteria: a) the Equivalent Number of Looks ($ENL = mean^2/variance$) > 2, and b) the Signal to additive Noise Ratio ($SNR_A = (mean - NESZ)/NESZ$)) > 1 [5]. The NESZ (Noise Equivalent Sigma Zero was estimated from the metadata of the image).

The CFAR algorithm is implemented by sliding across the sub-image a stencil window having at its center a test cell containing the pixel(s) under test (PUT), followed by a guard window isolating the central test cell from a background external window used to estimate the statistics of the sea clutter for the chosen pdf. The background, guard and test window sizes were set to, respectively, 100 × 100, 20 × 20 and 1 × 1. These values were set considering the pixel size and assuming 300m a typical size of the biggest ships to be searched. The CFAR was implemented based on the 3-parameter Generalized Gamma distribution - GΓD, used for the statistical modeling of intensity sigma-zero sea clutter values [6]. The GΓD parameters estimation was done analytically by an approximate estimator [7], based on the method of log-cumulants (MoLC). For an accepted False Alarm Rate – FAR, a threshold T must be determined for the pdf at each position of the stencil window. For the GΓD this estimation was done analytically as indicate in [8]. If central pixel value is larger than T, it is set to 1 and considered as positive detection; if equal or less than T, the central pixel is set to zero and assumed to be sea clutter. After running the CFAR stencil throughout the image a binary matrix image is generated. Statistical goodness-of-fit of GΓD was analyzed using Kolmogorov-Smirnov – KS distance [9].

3. RESULTS AND DISCUSSION

A. Wave age classification and comparison of GΓD fit

Fig. 1(a)-(c) shows sub-image examples for distinct *WA* classification. In general, the three *WA* classes are distinguishable by the presented ocean features. In young wind-sea conditions it is noticeable the presence of linear alternating darker and brighter features, of extension ~2 to 5 km, notably known as wind streaks, typical of ocean environments dominated by stronger winds. On the other hand, the swell sub-image exemplifies the case of longer period and wavelength waves of the order of hundreds of meters. In this case, these features are also related to bright and dark features, associated with wave crests and troughs. In between, the old wind-sea sub-image case represents a transitional environment, in which the waves are closer to fully development. In summary, the *WA* parameter seems appropriate as a simple and good criterion to separate distinct ocean environments integrating wind and wave data and, thus, be used to assess the GΓD fitting general behavior.

Examples of GΓD fitting results for the three WA classes are presented in Fig. 2(a)-(f). For detailed display purposes, right column shows the histogram regions normalized by their mean (σ^o/M) and displayed in semi-log scale. It is observed that GΓD has a better fit for young wind-sea conditions. As WA increases, the theoretical PDF values are seen to underestimate the observed data, particularly for higher values of σ^o, as exemplified starting from the point indicated by the red arrow on Fig. 2(e). As shown in Table I, this is also confirmed by KS distance results for all selected sub-images. The mean KS distances indicate that GΓD ability of fitting is worse at swell conditions, i.e., with presence of long period waves. As a result, a higher quantity of false alarms is expected to occur on CFAR detection as WA increases, due to the PDF sub-estimations.

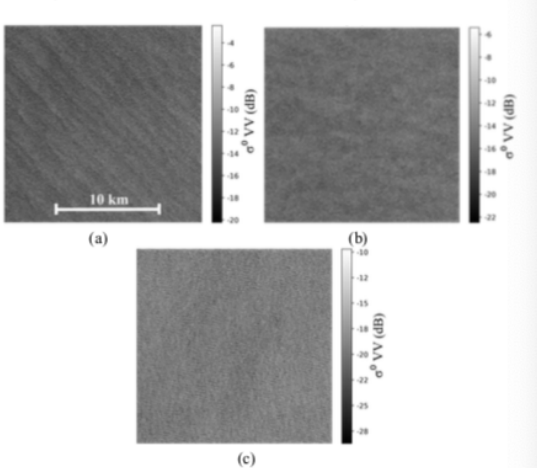

Fig. 1 Wave Age sub-image examples at mid-range incidence angles and for (a) Young wind-sea, (b) old wind-sea, and (c) swell.

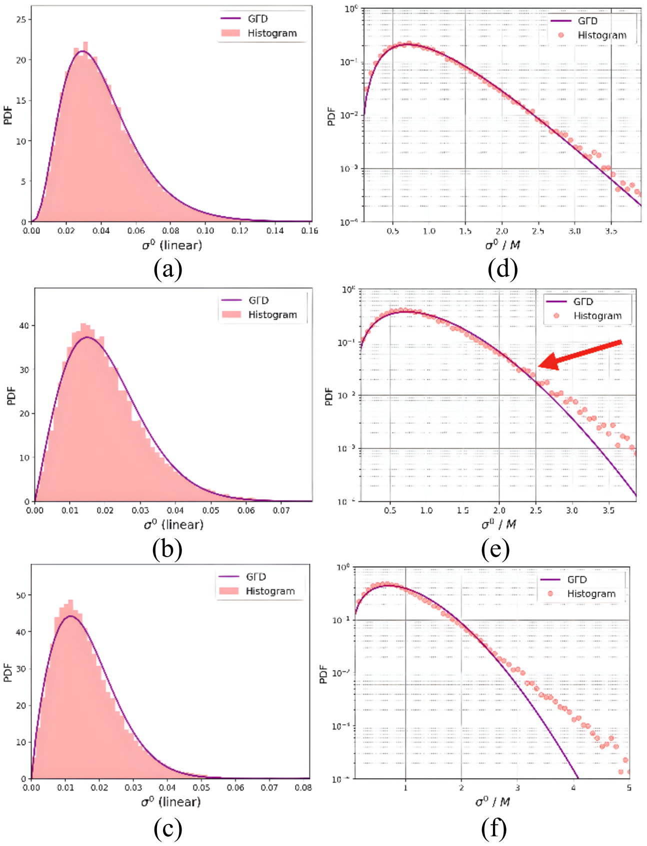

Fig. 2 Comparison of GGD fitting results for WA classes. (a)-(c) Image histograms. (d)-(f) Image histograms normalized. Each row represents young wind-sea, old wind-sea and swell, respectively.

As indicated, a sub-estimation of observed values by the pdf will result in an increase of false alarms – FA, due to a smaller threshold than what it should be from a perfect fit. Therefore, the observed number of FA is expect being higher than the theoretical one associated to the chosen FAR. As an example, for an assumed probability of false alarm - PFA of 10^{-4}, in our image of 667x667 pixels (444,889 pixels), 44 false positives pixels should be expected. To consider this problem, the following correction parameter f and equation is suggested [10],

$$T_A = (T - M).f + M$$

Where T is the theoretical threshold, derived from the adjusted pdf, M is the mean value of σ^o, and T_A is the corrected value of T. A f=1 corresponds to a zero correction.

TABLE I
KOLMOGOROV-SMIRNOV DISTANCE RESULTS (N=26657)

***WA* class**	**Radar range**	**N. of subimages**	**Mean KS distance**
Young wind-sea	Near-range	308	**0.059**
	Mid-range	479	**0.056**
	Far-range	619	**0.056**
Old wind-sea	Near-range	5600	**0.060**
	Mid-range	8227	**0.060**
	Far-range	8102	**0.060**
Swell	Near-range	958	**0.063**
	Mid-range	1273	**0.063**
	Far-range	1091	**0.064**

The strategy adopted to estimate de f values for different WA image classes was to vary f from unity onward in small increments and compare the number of false alarms N_{FA} observed to the expected one which is dependent on the FAR chosen. The derived f value is that one which makes both the observed and expected number of false alarms equal. Fig. 3 illustrate the results obtained.

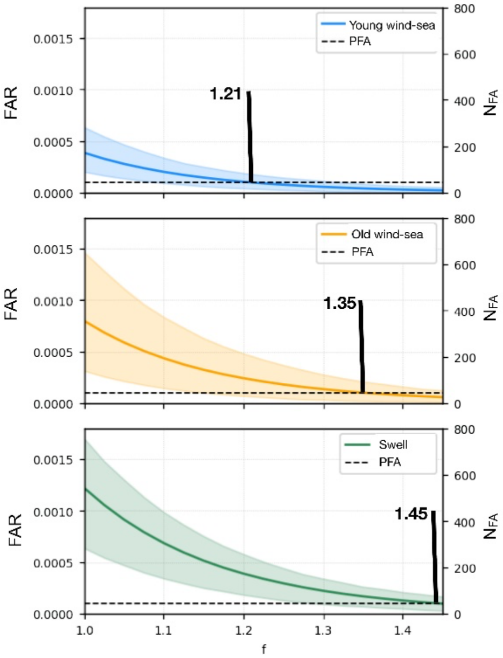

Fig. 3 Observed FAR as a function of adjustment factor f for a PFA=10^{-4}. Dashed horizontal line corresponds to the expected number of false alarms (right vert. axis). Color bands are the 10% to 90% percentiles for different WA classes. Solid color lines are the average values. Vertical black line indicates the optimal f value.

The Table II shows the f optimal values derived for different WA classes and PFA.

PFA	**Young wind-sea**	**Old wind-sea**	**Swell**
10^{-2}	1.07	1.12	1.18
10^{-3}	1.14	1.25	1.32
10^{-4}	1.21	1.35	1.45
10^{-5}	1.32	1.52	1.65
10^{-6}	1.49	1.80	1.90

Table II. Adjustment f values derived for distinct WA classes and FFA.

Considering the spatial resolution of the image (30m) and the typical sizes of ships to be detected, it is expected that the number of positive pixels be relatively larger than the number of ships detected, even for a perfect CFAR detection. Additionally, the number of positive alarmed pixels is a function of the PFA chosen. So, for a better evaluation of the CFAR performance we made a clustering of detected neighboring pixels. The binary images were transformed in vectorial files (shapefiles) using the gdal polygonise function of GDAL7 library. From this, the CFAR performance was evaluated by these vector elements of detection, not the number of pixels.

Method	**Ships present**	8
CFAR	**Total detections**	690
	True detections	8
	False alarms	682
	Lost ships	0
CFAR+ f correction	**Total detections**	39
	True detections	8
	False alarms	31
	Lost ships	0

Table III. Elements of ship detection for a group of 6 sub-images and for the swell class and a PFA=10^{-6}.

In Table III we illustrate the case for the worst environmental scenario of WA>35 swell waves, and for a PFA = 10^{-6}, with and without the threshold f adjustment. These numbers refer to the total number of pixels and clusters determined for the six images analyzed. A first point to notice is the large number of positive and false alarm detections without f adjustment. With the f adjustment, the number of false positives was reduced to less than 6% of the original, showing the efficacy of the adjustment. The total number of only 8 ships present is the number in the AIS system for the region and period. This could be, however, an underestimation of the true value considering that an unknown number of ships could be either not transmitting, or not having any AIS equipment installed on board. Another point to be noticed is that for large metallic objects such big ships, their strong backscatter frequently produces “ghost” detections in pairs around the true ship and oriented mostly in the azimuthal direction, for which they are called as azimuthal ambiguities.

Therefore, for one real ship we might have three detections: one real and two ghost images. For very weak winds, these ambiguities tend to be more prominent in relation to the sea clutter and being wrongly detected by the CFAR, even for a very small PFA [12].

4. CONCLUSIONS

We showed in this paper the important role that the environmental conditions at sea might play in affecting the accuracy and efficacy of ship detection done for SAR images and using the CFAR statistical algorithm. As presented, even with the use of a sophisticated three parameter pdf (Generalized Gamma) which is acknowledged as very flexible and showing good fitting results to the sigma zero SAR data, the presence of surface waves, and in particular waves with high Wave Age (old wind-sea and swell), makes it difficult to properly adjust the GΓD parameters so as to obtain a good overall fit of the theoretical function to the observed data. This is particularly serious for the higher values of the distribution, just the area of the pdf where the threshold normally is located and used for comparing with also high return values of ships.

As it was presented, if not adjusted, the number of false positives might be too high to be acceptable, even for a very small PFA. It was shown that a very high reduction of FA can be accomplished by using the proposed values of the f adjustment factor for the threshold. We presented a table of f values to be used as a function of the three WA categories; young wind-sea, old wind-sea and swell waves.

This paper was prepared as part of the Project CNPq/MCTI 06/2020 – Pesquisa e Desenvolvimento para Enfrentamento de Derramamento de Óleo na Costa Brasileira – Programa Ciência no Mar. Processo CNPq No 440857/2020-1.

REFERENCES

[1] K. El-Darymli et al. Target detection in synthetic aperture radar imagery: a state-of-art survey. J. Applied Rem. Sens., v. 7, 1-35, 2013.

[2] K. Ouchi. Current Status on Vessel Detection and Classification by Synthetic Aperture Radar for Maritime Security and Safety. The 38th Symposium on Remote Sensing for Environmental Sciences 3 – 5 September, Japan, 2016.

[3] H. Hersbach et al. The ERA5 global reanalysis. Quart. J. Royal Met. Soc., v. 146, no. 730, 1999-2049, 2020.

[4] G. J. Komen et al. Dynamics and Modelling of Ocean Waves. Cambridge Univ. Press, New York, 1994.

[5] M. M. Espeseth et al. The impact of system noise in polarimetric SAR imagery on oil spill observations. IEEE Trans. Geos. Rem. Sens., v. 58, no. 6, 4194–4214, 2020.

[6] H. Li, W. Hong, Y. Wu and P. Fan. On the empirical-statistical modeling of SAR images with Generalized Gamma Distribution. IEEE J. Sel. Top. Signal. Proc., v. 5, 386-397, 2011.

[7] G. Gao et al. Scheme of parameter estimation for Generalized Gamma Distribution and its application to ship detection in SAR images. IEEE Trans. Geosc. and Remote Sens., v. 55, 1812-1836, 2017.

[8] Sun et al. The dependence of sea SAR image distribution parameters on surface wave characteristics. Rem. Sens., v. 10, 1–18, 2018.

[9] M. D. DeVore and J. A. O'Sullivan. Quantitative statistical assessment of conditional models for synthetic aperture radar. IEEE Trans. Im. Proces., v. 13, 113-125, 2004.

[10] Greidanus et al. The SUMO ship detector algorithm for satellite radar images. Remote Sensing, v. 9, 1-27, 2017.

[11] GDAL - Geospatial Data Abstraction Library: <https://gdal.org/programs/gdal_polygonize.html>. Acess in 10/18/2021.

[12] D. Velotto et al. Azimuth ambiguities removal for ship detection using full polarimetric X-band SAR data. IEEE Transactions on Geoscience and Remote Sensing, v. 52, 76–88, 2014.